Available online at www.sciencedirect.com
SCIENCE DIRECT®
Journal of Sound and Vibration 289 (2006) 77–93
JOURNAL OF SOUND AND VIBRATION
www.elsevier.com/locate/jsvi

Thermal postbuckling and vibration analyses of functionally graded plates

Jae-Sang Park, Ji-Hwan Kim*

School of Mechanical and Aerospace Engineering, Seoul National University, San 56-1, Sillim-Dong, Gwanak-Gu, Seoul 151-742, Republic of Korea

Received 14 May 2004; received in revised form 29 December 2004; accepted 29 January 2005
Available online 12 April 2005

Abstract

Thermal postbuckling and vibration behaviors of the functionally graded (FG) plate are investigated. The material properties of the FG plate are assumed to vary continuously through the thickness of the plate and as temperature with the nonlinearity. The nonlinear finite element equations based on the first-order shear deformation plate theory are formulated for the FG plate. The von Karman nonlinear strain–displacement relationship is used to account for the large deflection of the plate. The incremental form considering the initial displacement and initial stress is adopted for the nonlinear temperature-dependent material properties of the functionally graded material. The numerical result shows the characteristics of the thermal postbuckling and vibration of the FG plate in the pre- and post-buckled regions.

1. Introduction

Functionally graded materials (FGMs) are the advanced composites which have continuously varying material composition and properties through certain dimension of the structure to achieve the desired goals. Because the fiber-reinforced composites have a mismatch of material properties across an interface of two discrete materials bonded together, there could be the severe thermal

*Corresponding author. Tel.: +82 2 880 7383; fax: +82 2 887 2662.
E-mail address: jwhkim@snu.ac.kr (J.-H. Kim).

0022-460X/$ - see front matter © 2005 Elsevier Ltd. All rights reserved.
doi:10.1016/j.jsv.2005.01.031

stress concentration phenomena at the interface of the fiber-reinforced composites. However, by gradually varying the material properties of FGMs, this problem can be avoided or reduced. Therefore, FGMs with a mixture of the ceramic and metal are applied to the thermal barrier structures for the space shuttle, combustion chamber and nuclear plants, etc.

Reddy [1] researched the linear and nonlinear static analyses of the functionally graded (FG) plate under thermomechanical loads. Theoretical formulation, Navier's solution and finite element model for the FG plate were presented. Croce and Venini [2] performed the static analysis of the FG plate under the thermal and mechanical loads using the finite element method. The static and dynamic responses of the functionally graded ceramic-metal plate were investigated [3]. In their study, the response of the FG plate with material properties between those of the ceramic and metal was not intermediate to the response of the ceramic-metal plates. Cho and Oden [4] studied thermo-elastic characteristics of FGMs using Crank–Nicolson–Galerkin method. It was found that the FGMs show considerable improvement in the temperature and thermal stress distributions. Woo and Meguid [5] performed the nonlinear static analysis for the FG plate and shallow shell under the mechanical load and a temperature field. Yang and Shen [6] investigated the nonlinear bending behavior of the FG plate subjected to the uniform load with the temperature rise. In their research, material properties of the FG plate were assumed to be dependent on the position and temperature. Javaheri and Eslami [7] studied the thermal buckling of the FG plate using the analytical solution based on the classical plate theory. Lanhe [8] presented the analytical solution for the thermal buckling of the thick FG plate. Na and Kim [9] researched three-dimensional thermal buckling analysis of the FG plate using the assumed strain mixed formulation. Eighteen-node solid elements were adopted to account for the variation of material properties and temperature field along the thickness direction. The three-dimensional exact solution for the vibration analysis of the FG plate was presented [10]. Pradhan et al. [11] studied vibration characteristics of the FG shells using Rayleigh method. Natural frequencies of the FG shells were observed to be dependent on the constituent volume fraction. Yang and Shen [12] investigated the free and forced vibration problems for the initially stressed FG plate in the thermal environment. Material properties of FGMs are assumed to be temperature dependent and graded in the thickness direction. Their results show that the plates with intermediate material properties do not necessarily have intermediate dynamic response. Kitipornchai et al. [13] studied the nonlinear vibration of imperfect FGM plates based on Reddy's higher-order shear deformation plate theory using semi-analytical solution. Material properties were assumed to be temperature dependent in their paper. Yang et al. [14] showed the influences of FG material composition and temperature change on the dynamic stability, buckling and vibration of FGM plates. He et al. [15] researched the active control of the FG plate using piezoelectric sensors and actuators. Liew et al. [16] investigated postbuckling characteristics of piezoelectric FGM plates with various applied voltage, inplane forces, volume fraction exponents and temperature. Averill and Reddy [17] studied the nonlinear response of laminated composite panels subjected to thermal loads using the refined theory and finite element method. Zhou et al. [18] investigated the vibration of the thermally buckled composite plate. The initial deflection was considered, and triangular elements were used for the finite element method based on the classical plate theory. Lee and Lee [19] studied the vibration of the thermally postbuckled composite plate using the first-order shear deformation plate theory (FSDT). Park et al. [20] performed the vibration analysis of the thermally postbuckled composite plate embedded with shape memory alloy (SMA)

fibers. To account for the temperature-dependent material properties of SMA fibers, the incremental method considering the initial displacement and initial stress was adopted.

However, there have been few researches dealing with characteristics for the thermal postbuckling and vibration of the FG plate considering the nonlinear temperature-dependent material properties. Therefore, in this study, the nonlinear finite element equations based on the FSDT are formulated for the FG plate under thermal loads. The von Karman nonlinear strain–displacement relationship is used to account for the thermal large deflection. The incremental form considering the initial displacement and initial stress is adopted for the nonlinear temperature-dependent material properties of FGMs. The numerical results show the characteristics of the thermal postbuckling and vibration of the pre- and post-buckled FG plate.

2. Nonlinear finite element formulation

2.1. Incremental method

The temperature rise $\mathrm{d}T$ from the reference temperature T_{ref} to the current temperature T can be divided by many and small temperature increment ΔT as shown in Fig. 1(a). The small temperature increment is defined as $\Delta T = T - T_0$, where the subscript '0' means the initial state. It can be assumed that the temperature-dependent properties are constant with the values at the current temperature T during the small temperature increment. As shown in Fig. 1(b), the governing equation for the given temperature increment ΔT is derived considering the initial displacement and initial stress.

2.2. Incremental strain–displacement relationship

The von Karman nonlinear incremental strain–displacement relationship for the FSDT can be written as follows [20]:

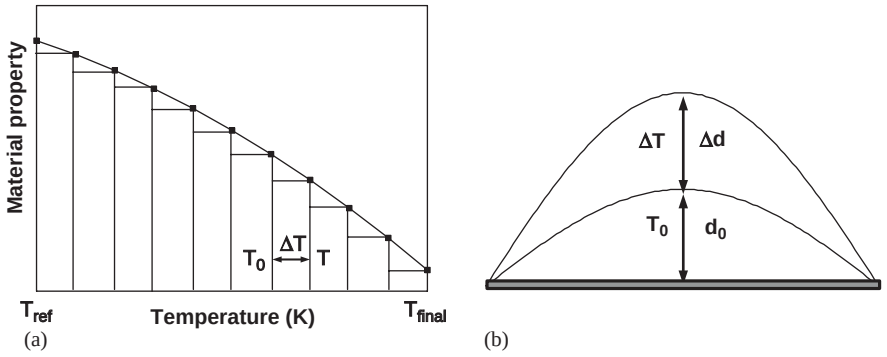

Fig. 1. (a) Definition of temperature increment; (b) incremental displacement of the FG plate.

The incremental inplane strain vector is

$$\Delta\mathbf{e} = \begin{Bmatrix} \Delta\varepsilon_{xx} \\ \Delta\varepsilon_{yy} \\ \Delta\gamma_{xy} \end{Bmatrix} = \begin{Bmatrix} \dfrac{\partial\Delta u}{\partial x} \\ \dfrac{\partial\Delta v}{\partial x} \\ \dfrac{\partial\Delta u}{\partial y} + \dfrac{\partial\Delta v}{\partial x} \end{Bmatrix} + \frac{1}{2}\begin{Bmatrix} \left(\dfrac{\partial\Delta w}{\partial x}\right)^2 \\ \left(\dfrac{\partial\Delta w}{\partial x}\right)^2 \\ 2\left(\dfrac{\partial\Delta w}{\partial x}\right)\left(\dfrac{\partial\Delta w}{\partial y}\right) \end{Bmatrix} + \begin{Bmatrix} \dfrac{\partial\Delta w}{\partial x}\dfrac{\partial w_0}{\partial x} \\ \dfrac{\partial\Delta w}{\partial y}\dfrac{\partial w_0}{\partial y} \\ \dfrac{\partial\Delta w}{\partial x}\dfrac{\partial w_0}{\partial y} + \dfrac{\partial w_0}{\partial x}\dfrac{\partial\Delta w}{\partial y} \end{Bmatrix} + z\begin{Bmatrix} \dfrac{\partial\Delta\theta_x}{\partial x} \\ \dfrac{\partial\Delta\theta_y}{\partial y} \\ \dfrac{\partial\Delta\theta_x}{\partial y} + \dfrac{\partial\Delta\theta_y}{\partial x} \end{Bmatrix} \tag{1a}$$

or

$$\Delta\mathbf{e} = \Delta\boldsymbol{\varepsilon}_m + \Delta\boldsymbol{\varepsilon}_\theta + \Delta\boldsymbol{\varepsilon}_0 + z\Delta\boldsymbol{\kappa} = \Delta\boldsymbol{\varepsilon} + z\Delta\boldsymbol{\kappa}, \tag{1b}$$

where $\Delta\boldsymbol{\varepsilon}_m$, $\Delta\boldsymbol{\varepsilon}_\theta$, $\Delta\boldsymbol{\varepsilon}_0$ and $\Delta\boldsymbol{\kappa}$ are the incremental inplane linear strain vector, the incremental nonlinear strain vector, the incremental inplane strain vector due to the initial deflection and the incremental curvature strain vector, respectively. As shown in Eq. (1a), the incremental inplane strain consists of the incremental displacement Δu, Δv and Δw, the incremental rotation $\Delta\theta_x$ and $\Delta\theta_y$ and the initial deflection w_0.

In addition, the incremental transverse shear strain vector can be expressed as

$$\Delta\boldsymbol{\gamma} = \begin{Bmatrix} \Delta\gamma_{yz} \\ \Delta\gamma_{xz} \end{Bmatrix} = \begin{Bmatrix} \dfrac{\partial\Delta w}{\partial y} + \Delta\theta_y \\ \dfrac{\partial\Delta w}{\partial x} + \Delta\theta_x \end{Bmatrix}. \tag{2}$$

2.3. FGM material properties

By the power law, the volume fraction for the ceramic-metal FGM is given as

$$V_c(z) = \left(\frac{z}{h} + \frac{1}{2}\right)^k \quad (0 \leqslant k < \infty), \tag{3a}$$

$$V_c(z) + V_m(z) = 1, \tag{3b}$$

where V and k are the volume fraction of the constituent material and volume fraction index for the ceramic, respectively. In addition, subscripts 'c' and 'm' indicate the ceramic and metal, respectively. Fig. 2 shows the distribution of the volume fraction V_c through the plate thickness for various of the volume fraction index for the ceramic k.

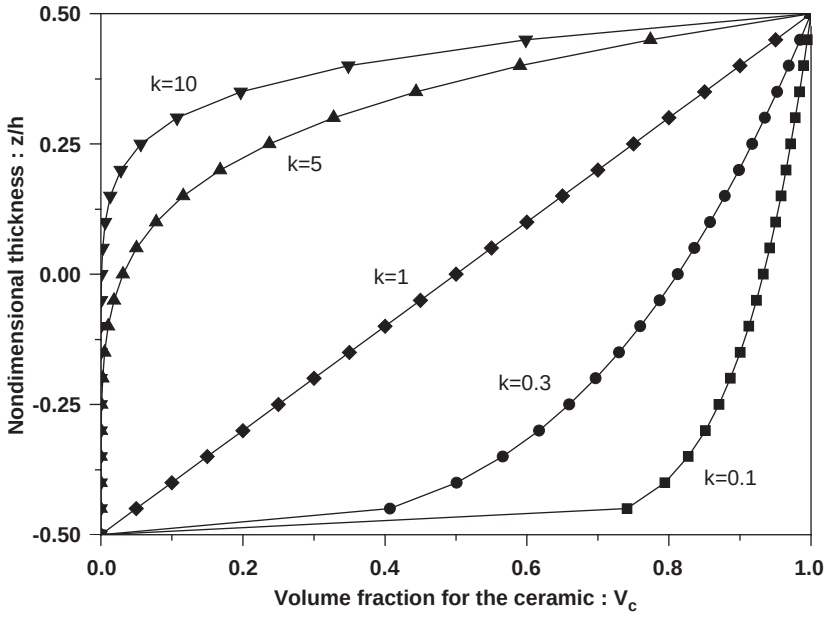

Fig. 2. Variation of volume fraction V_c through the plate thickness for various values of the volume fraction index k.

Material properties of FGMs can be written as [12]

$$P(z,T) = (P_c(T) - P_m(T))V_c(z) + P_m(T), \tag{4a}$$

$$P_c(T) \quad \text{or} \quad P_m(T) = P_0(P_{-1}T + 1 + P_1T + P_2T^2 + P_3T^3), \tag{4b}$$

where P is the effective material property. P_0, P_{-1}, P_1, P_2 and P_3 are the coefficients of temperature. Therefore, material properties such as Young's modulus, the thermal expansion coefficient and the density of FGMs can be calculated using Eq. (4). However, in this study, Poisson's ratio is assumed to be constant as $v = 0.3$. Material properties of FGMs vary continuously through the thickness of the plate and as temperature with the nonlinearity, as shown in Eqs. (3) and (4).

2.4. Constitutive equation

The constitutive equation for the FG plate during the small temperature increment can be expressed as [20]

$$\begin{Bmatrix} \mathbf{N} \\ \mathbf{M} \end{Bmatrix} = \begin{bmatrix} \mathbf{A} & \mathbf{B} \\ \mathbf{B} & \mathbf{D} \end{bmatrix} \begin{Bmatrix} \Delta\boldsymbol{\varepsilon} \\ \Delta\boldsymbol{\kappa} \end{Bmatrix} - \begin{Bmatrix} \mathbf{N}_{\Delta T} \\ \mathbf{M}_{\Delta T} \end{Bmatrix} + \begin{Bmatrix} \mathbf{N}_0 \\ \mathbf{M}_0 \end{Bmatrix}, \tag{5a}$$

$$\mathbf{Q} = \mathbf{A}_s\Delta\boldsymbol{\gamma} + \mathbf{Q}_0, \tag{5b}$$

where $\mathbf{A}$, $\mathbf{B}$, $\mathbf{D}$ and $\mathbf{A}_s$ are the inplane, bending–stretching coupling, bending and transverse shear stiffness matrices, respectively. $\mathbf{N}$, $\mathbf{M}$ and $\mathbf{Q}$ are the resultant vectors of the inplane force,

moment and transverse shear, respectively. Further, $\mathbf{N}_{\Delta T}$ and $\mathbf{M}_{\Delta T}$ are the thermal inplane force and thermal moment due to the incremental temperature ΔT, respectively. $\mathbf{N}_0$, $\mathbf{M}_0$ and $\mathbf{Q}_0$ are the inplane force, moment and transverse shear force due to the initial stress, respectively.

2.5. Governing equation

By using the principle of the virtual work and Eqs. (1), (2) and (5), the governing equation of the FG plate under thermal loads can be derived as follows:

$$\delta W = \delta W_{\text{int}} - \delta W_{\text{ext}} = 0. \tag{6}$$

The variation of the internal virtual work δW_{int} is given as

$$\begin{aligned}\delta W_{\text{int}} &= \int_A [\delta\boldsymbol{\varepsilon}^{\mathrm{T}}\mathbf{N} + \delta\boldsymbol{\kappa}^{\mathrm{T}}\mathbf{M} + \delta\boldsymbol{\gamma}^{\mathrm{T}}\mathbf{Q}]\,\mathrm{d}A \\ &= \delta\mathbf{d}^{\mathrm{T}}(\mathbf{K} - \mathbf{K}_{\Delta T} + \mathbf{K}_0 + \mathbf{K}_{w0} + \tfrac{1}{2}\mathbf{KN1}_{w0} + \tfrac{1}{2}\mathbf{KN1} + \tfrac{1}{3}\mathbf{KN2})\Delta\mathbf{d} \\ &\quad - \delta\mathbf{d}^{\mathrm{T}}\mathbf{P}_{\Delta T} + \delta\mathbf{d}^{\mathrm{T}}\mathbf{P}_0 - \delta\mathbf{d}^{\mathrm{T}}\mathbf{P}_{w0_{\Delta T}} + \delta\mathbf{d}^{\mathrm{T}}\mathbf{P}_{0_{w0}},\end{aligned} \tag{7}$$

where $\mathbf{d} = [u\ \ v\ \ \theta_x\ \ \theta_y\ \ w]^{\mathrm{T}}$ is the displacement vector. $\mathbf{K}$, $\mathbf{K}_{\Delta T}$, $\mathbf{K}_0$ and $\mathbf{K}_{w_0}$ are the linear stiffness matrix, the incremental thermal geometric stiffness matrix, the geometric stiffness matrix due to the initial stress and the initial deflection linear stiffness matrix, respectively. $\mathbf{KN1}_{w_0}$ is the first-order nonlinear mixed stiffness matrix which depends on the initial deflection and the first-order nonlinear incremental term. **KN1** and **KN2** are the first- and second-order nonlinear incremental stiffness matrices, respectively. In addition, $\mathbf{P}_{\Delta T}$, $\mathbf{P}_0$, $\mathbf{P}_{w0_{\Delta T}}$ and $\mathbf{P}_{0_{w0}}$ are the incremental thermal load vector, the initial stress load vector, the incremental thermal load vector due to the initial deflection and the load vector due to the initial load and initial deflection, respectively. There are the detailed derivations for the stiffness matrices and load vectors in Appendix A.

On the other hand, the variation of the external virtual work δW_{ext} is given as

$$\begin{aligned}\delta W_{\text{ext}} &= \int_A \begin{bmatrix} -I_0(\ddot{u}\delta u + \ddot{v}\delta v + \ddot{w}\delta w) - I_1(\ddot{\theta}_x\delta u + \ddot{u}\delta\theta_x + \ddot{\theta}_y\delta v + \ddot{v}\delta\theta_y) \\ -I_2(\ddot{\theta}_x\delta\theta_x + \ddot{\theta}_y\delta\theta_y) \end{bmatrix} \mathrm{d}A \\ &= -\delta\mathbf{d}^{\mathrm{T}}\mathbf{M}\Delta\ddot{\mathbf{d}},\end{aligned} \tag{8}$$

where $(I_0, I_1, I_2) = \int_{-h/2}^{h/2} \rho(1, z, z^2)\,\mathrm{d}z$ and h denotes the thickness of the plate. In addition, $\mathbf{M}$ is the mass matrix.

By substituting Eqs. (7) and (8) into Eq. (6), the governing equation for the FG plate under thermal loads can be obtained as

$$\begin{aligned}&\mathbf{M}\Delta\ddot{\mathbf{d}} + (\mathbf{K} - \mathbf{K}_{\Delta T} + \mathbf{K}_0 + \mathbf{K}_{w0} + \tfrac{1}{2}\mathbf{KN1}_{w0} + \tfrac{1}{2}\mathbf{KN1} + \tfrac{1}{3}\mathbf{KN2})\Delta\mathbf{d} \\ &\quad = \mathbf{P}_{\Delta T} - \mathbf{P}_0 + \mathbf{P}_{w0_{\Delta T}} - \mathbf{P}_{0_{w0}}.\end{aligned} \tag{9}$$

3. Solution procedures

The solution of Eq. (9) is assumed to be as

$$\Delta\mathbf{d} = \Delta\mathbf{d}_s + \mathbf{d}_t, \tag{10}$$

where $\Delta\mathbf{d}_s$ is the time-independent particular solution which means the incremental thermal large deflection, and $\mathbf{d}_t$ is the time-dependent homogeneous solution with small magnitude at the buckled position of $\mathbf{d}_0 + \Delta\mathbf{d}_s$.

Two sets of equations can be obtained by substituting Eq. (10) into Eq. (9) as

$$\begin{aligned}&(\mathbf{K} - \mathbf{K}_{\Delta T} + \mathbf{K}_0 + \mathbf{K}_{w0} + \tfrac{1}{2}\mathbf{KN1}_{w0_s} + \tfrac{1}{2}\mathbf{KN1}_s + \tfrac{1}{3}\mathbf{KN2}_s)\Delta\mathbf{d}_s \\ &\quad = \mathbf{P}_{\Delta T} - \mathbf{P}_0 + \mathbf{P}_{w0_{\Delta T}} - \mathbf{P}_{0_{w0}},\end{aligned} \tag{11a}$$

$$\mathbf{M}\ddot{\mathbf{d}}_t + (\mathbf{K} - \mathbf{K}_{\Delta T} + \mathbf{K}_0 + \mathbf{K}_{w0} + \mathbf{KN1}_{w0_s} + \mathbf{KN1}_s + \mathbf{KN2}_s)\mathbf{d}_t = \mathbf{0}. \tag{11b}$$

Eqs. (11) are equations for the thermal postbuckling and vibration analyses of the thermally postbuckled plate. Further, the subscripts 's' and 't' denote the static and dynamic displacement, respectively.

3.1. Thermal postbuckling problem

Newton–Raphson iterative method is adopted to solve the thermal postbuckling displacement. Introducing the function $\mathbf{\Psi}(\Delta\mathbf{d}_s)$ to Eq. (11a) as,

$$\begin{aligned}\mathbf{\Psi}(\Delta\mathbf{d}_s) = &(\mathbf{K} - \mathbf{K}_{\Delta T} + \mathbf{K}_0 + \mathbf{K}_{w0} + \tfrac{1}{2}\mathbf{KN1}_{w0_s} + \tfrac{1}{2}\mathbf{KN1}_s + \tfrac{1}{3}\mathbf{KN2}_s)\Delta\mathbf{d}_s \\ &- \mathbf{P}_{\Delta T} + \mathbf{P}_0 + \mathbf{P}_{w0_{\Delta T}} + \mathbf{P}_{0_{w0}} = \mathbf{0}.\end{aligned} \tag{12}$$

The tangent stiffness matrix and unbalance load vector for Newton–Raphson iterative method can be written using above function $\mathbf{\Psi}(\Delta\mathbf{d}_s)$ as

For the ith iteration,

$$\mathbf{K}_{\tan_i} = \left[\frac{\mathrm{d}(\mathbf{\Psi}(\Delta\mathbf{d}_s))}{\mathrm{d}(\Delta\mathbf{d}_s)}\right]_i = (\mathbf{K} - \mathbf{K}_{\Delta T} + \mathbf{K}_0 + \mathbf{K}_{w0} + \mathbf{KN1}_{w0_s} + \mathbf{KN1}_s + \mathbf{KN2}_s)_i \tag{13a}$$

and

$$\begin{aligned}\mathbf{\Psi}(\Delta\mathbf{d}_s)_i = &\left(\mathbf{K} - \mathbf{K}_{\Delta T} + \mathbf{K}_0 + \mathbf{K}_{w0} + \tfrac{1}{2}\mathbf{KN1}_{w0_s} + \tfrac{1}{2}\mathbf{KN1}_s + \tfrac{1}{3}\mathbf{KN2}_s\right)_i\Delta\mathbf{d}_{s_i} \\ &- \mathbf{P}_{\Delta T} + \mathbf{P}_0 + \mathbf{P}_{w0_{\Delta T}} + \mathbf{P}_{0_{w0}}.\end{aligned} \tag{13b}$$

Therefore, Eq. (11a) can be written as

$$\mathbf{K}_{\tan_i}\delta\mathbf{d}_{s_{i+1}} = -\mathbf{\Psi}(\Delta\mathbf{d}_s)_i. \tag{14}$$

The incremental displacement is updated as

$$\Delta\mathbf{d}_{s_{i+1}} = \Delta\mathbf{d}_{s_i} + \delta\mathbf{d}_{s_{i+1}}. \tag{15}$$

It is considered that the incremental displacement is converged when the maximum value of $\|\delta\mathbf{d}_{s_{i+1}}\|$ is less than 10^{-6}. In addition, the thermal postbuckling displacement is calculated using

the converged incremental displacement as

$$\mathbf{d}_s = \mathbf{d}_0 + \Delta\mathbf{d}_s. \tag{16}$$

3.2. Vibration problem

After the thermal postbuckling displacement is calculated from the thermal postbuckling analysis, the vibration analysis is performed at the updated equilibrium position of $\mathbf{d}_0 + \Delta\mathbf{d}_s$.

Because the sum of stiffness matrices of Eq. (11b) equals the tangent stiffness matrix with the converged displacement in Eq. (14), therefore, Eq. (11b) can be expressed as

$$\begin{aligned}&\mathbf{M}\ddot{\mathbf{d}}_t + (\mathbf{K} - \mathbf{K}_{\Delta T} + \mathbf{K}_0 + \mathbf{K}_{w0} + \mathbf{KN1}_{w0_s} + \mathbf{KN1}_s + \mathbf{KN2}_s)\mathbf{d}_t \\ &\quad = \mathbf{M}\ddot{\mathbf{d}}_t + \mathbf{K}_{\tan}\mathbf{d}_t = \mathbf{0}.\end{aligned} \tag{17}$$

If the analyses for the thermal postbuckling and vibration at the thermally postbuckled state are completed during the given temperature increment, the initial displacement and initial stress are updated for the next temperature increment. These solution procedures are performed until the temperature reaches the final temperature.

4. Numerical results and discussions

In this section, the code verification and numerical analyses for the thermal postbuckling and vibration of the FG plate are performed using the finite element method (FEM). A uniform 6×6 mesh of nine noded elements is employed. To prevent the shear locking phenomena, the reduced integration technique is used to integrate terms related to the transverse shear stress.

4.1. Code verification

To verify the code used in this study, three examples are discussed. First, the thermal buckling analysis of all simply supported square FG plate is performed and compared with Ref. [7]. The ceramic is rich at the top and the metal is rich at the bottom of the FG plate. In this example, temperature-independent material properties are considered; Young's modulus and the thermal expansion coefficient for aluminum are $E_m = 70\,\text{GPa}$ and $\alpha_m = 23 \times 10^{-6}/^{\circ}\text{C}$ and for alumina are $E_c = 380\,\text{GPa}$ and $\alpha_c = 7.4 \times 10^{-6}/^{\circ}\text{C}$, respectively. Poisson's ratio v is assumed to be constant as 0.3. Fig. 3 shows that the present result using FEM has good agreement with the analytical solution of Ref. [7].

Second, the linear vibration analysis of all simply supported FG plate is performed for the two special cases of the isotropy. Table 1 represents the present result that agrees well with the result of Ref. [15].

Finally, to ensure the accuracy of the incremental method used in this study, the thermal postbuckling behavior of the composite plate using the incremental method is compared with the previous result of Ref. [17]. The thickness of a lamina is $1.25 \times 10^{-4}\,\text{m}$, the planar dimension of the square plate is 0.15 m, and the lay-up condition is $[45/-45/0/90]_s$. The boundary conditions

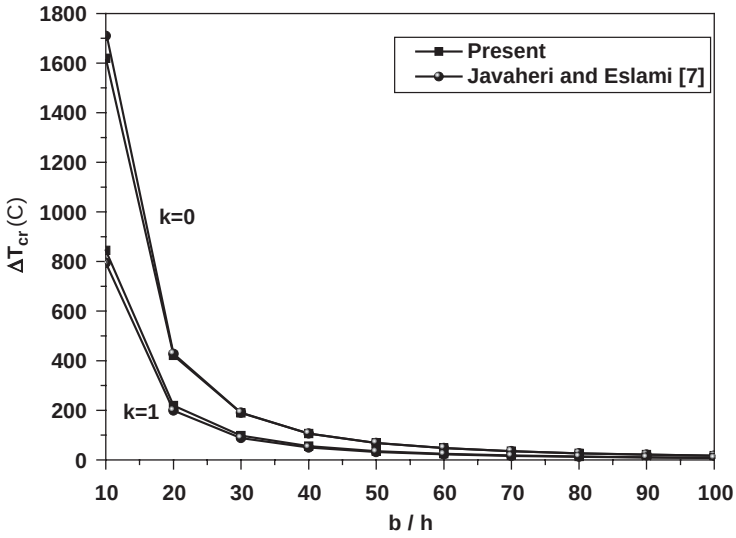

Fig. 3. Critical temperature change of the FG plate vs. b/h ($b/a = 1$).

Table 1
Natural frequency for simply supported FG plate for the two special cases of isotropy

Mode No.	Natural frequency (Hz)			
	$k = 0$		$k = 2000$	
	Present	Ref. [15]	Present	Ref. [15]
1	145.06	144.66	274.23	268.92
2	362.41	360.53	685.18	669.40
3	362.41	360.53	685.18	669.40
4	579.39	569.89	1095.40	1052.49
5	724.62	720.57	1369.98	1338.52

are all simply supported with the immovable inplane edges. The material properties are

$$E_1 = 155.0\,\text{GPa}, \quad E_2 = 8.07\,\text{GPa},$$
$$G_{12} = G_{13} = 4.55\,\text{GPa}, \quad G_{23} = 3.25\,\text{GPa},$$
$$v_{12} = 0.22, \quad \rho = 1586\,\text{kg/m}^3,$$
$$\alpha_1 = -0.07 \times 10^{-6}/^{\circ}\text{C}, \quad \alpha_2 = 30.1 \times 10^{-6}/^{\circ}\text{C}.$$

Fig. 4 shows that the present result using the incremental method has an excellent agreement with the result of Ref. [17].

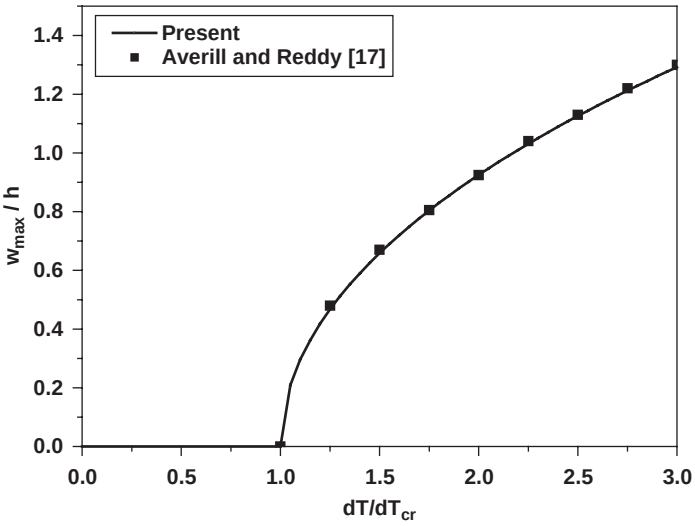

Fig. 4. Thermal postbuckling behavior of the composite plate.

Table 2
Material properties of ceramic and metal for two types of FGMs [12]

	Material	P_{-1}	P_0	P_1	P_2	P_3
E (Pa)	Si_3N_4	0	348.43×10^9	-3.070×10^{-4}	2.160×10^{-7}	-8.946×10^{-11}
	SUS304	0	201.04×10^9	3.079×10^{-4}	-6.534×10^{-7}	0
	Aluminum oxide	0	349.55×10^9	-3.853×10^{-4}	4.027×10^{-7}	-1.673×10^{-10}
	Ti-6A1-4V	0	122.56×10^9	-4.586×10^{-4}	0	0
ρ (kg/m^3)	Si_3N_4	0	2370	0	0	0
	SUS304	0	8166	0	0	0
	Aluminum oxide	0	3750	0	0	0
	Ti-6A1-4V	0	4429	0	0	0
α (1/K)	Si_3N_4	0	5.8723×10^{-6}	9.095×10^{-4}	0	0
	SUS304	0	12.330×10^{-6}	8.086×10^{-4}	0	0
	Aluminum oxide	0	6.8269×10^{-6}	1.838×10^{-4}	0	0
	Ti-6A1-4V	0	7.5788×10^{-6}	6.638×10^{-4}	-3.147×10^{-6}	0

4.2. Thermal postbuckling analysis

The thermal postbuckling behavior of the FG plate is studied. The ceramic is rich at the top and the metal is rich at the bottom of the FG plate. The planar dimension of the plate ($a \times b$) is 0.30×0.30 (m) and the thickness ratio (h/a) is 1/100. The simply supported boundary conditions are considered for all edges which are immovable for the inplane directions. Table 2 shows material properties for two types of FGMs used in this research. The uniform temperature change is applied to the plate, and the reference temperature T_{ref} is assumed to be 300 K.

Figs. 5–7 represent the thermal postbuckling behaviors of the Si_3N_4/SUS304 and aluminum oxide/Ti-6A1-4V FG plates. For the isotropic plates with Si_3N_4, SUS304, aluminum oxide and Ti-6A1-4V, thermal postbuckling behaviors are the bifurcation buckling behaviors that the thermal large deflection has suddenly occurred when the temperature reaches the critical temperature. However, for the Si_3N_4/SUS304 and aluminum oxide/Ti-6A1-4V FG plates, the thermal large deflection is increased monotonically as the temperature increases from the reference temperature. This is because the FG plate is the unsymmetric plate. It is well known that

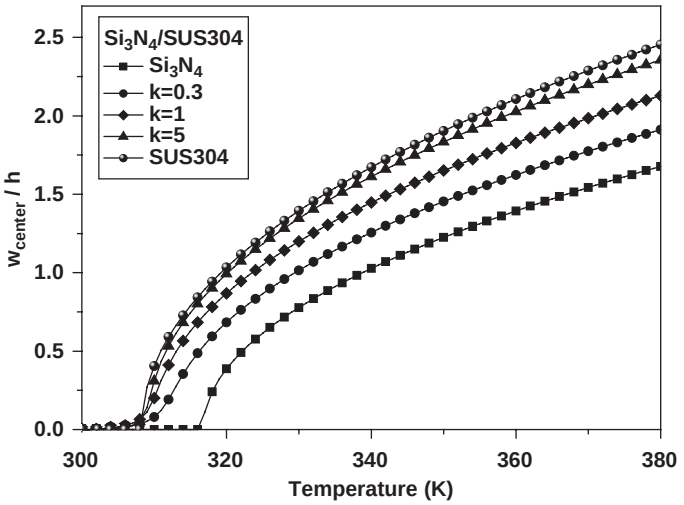

Fig. 5. Thermal postbuckling behavior of the Si_3N_4/SUS304 FG plate.

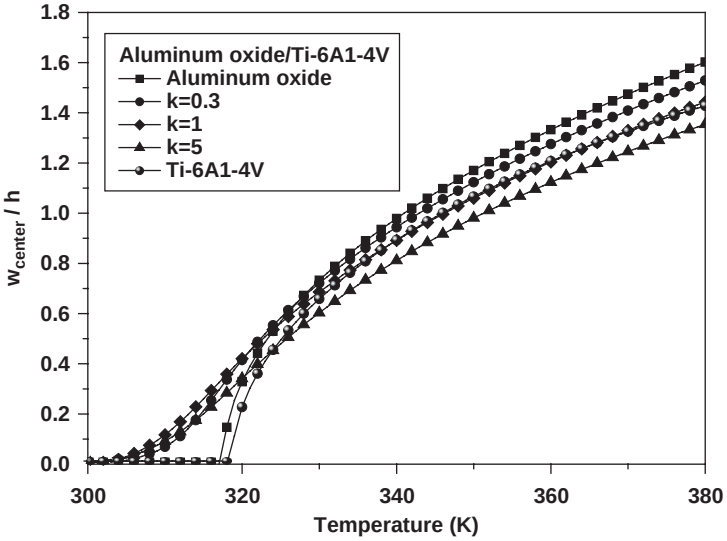

Fig. 6. Thermal postbuckling behavior of the aluminum oxide/Ti-6A1-4V FG plate.

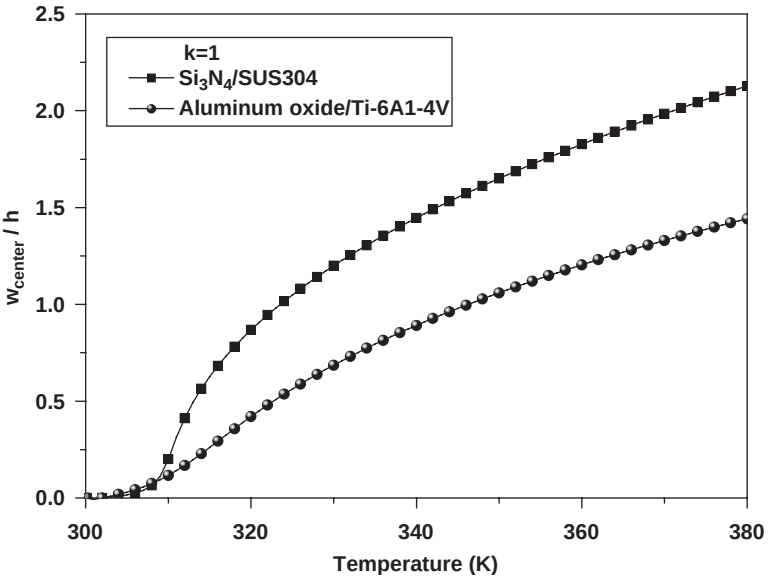

Fig. 7. Thermal postbuckling behaviors of the Si_3N_4/SUS304 and aluminum oxide/Ti-6A1-4V FG plates with $k = 1$.

the postbuckling behaviors for the isotropic and symmetric laminated composite plates are the bifurcation buckling behavior.

Fig. 5 shows the thermal postbuckling behaviors of the isotropic plates with Si_3N_4 and SUS304 and the Si_3N_4/SUS304 FG plates with $k = 0.3$, 1 and 5. The larger the volume fraction index for the ceramic k, the larger the thermal postbuckling deflection of the FG plate. In addition, there are the thermal postbuckling behaviors of the Si_3N_4/SUS304 FG plate between the thermal buckling behaviors of the isotropic plates with Si_3N_4 and SUS304.

Fig. 6 represents the thermal postbuckling behaviors of the isotropic plates with the aluminum oxide and Ti-6A1-4V and the aluminum oxide/Ti-6A1-4V FG plates with $k = 0.3$, 1 and 5. The temperature–displacement relationship of the aluminum oxide/Ti-6A1-4V FG plate is similar with that of the Si_3N_4/SUS304 FG plate, however, unlike the thermal postbuckling behavior of the Si_3N_4/SUS304 FG plate, the larger the volume fraction index for the ceramic k, the smaller the thermal postbuckling deflection of the FG plate. In addition, there are no thermal postbuckling behaviors of the aluminum oxide/Ti-6A1-4V plate between the thermal buckling behaviors of the isotropic plates with the aluminum oxide and Ti-6A1-4V. Fig. 7 shows the thermal postbuckling behaviors of the Si_3N_4/SUS304 and aluminum oxide/Ti-6A1-4V FG plates for $k = 1$. The thermal large deflection of the FG plate with aluminum oxide/Ti-6A1-4V is lower than that with Si_3N_4/SUS304.

4.3. Vibration analysis

Figs. 8–10 represent the vibration behaviors of the FG plates in the pre- and post-buckled regions for the thermal postbuckling behaviors discussed in Section 4.2.

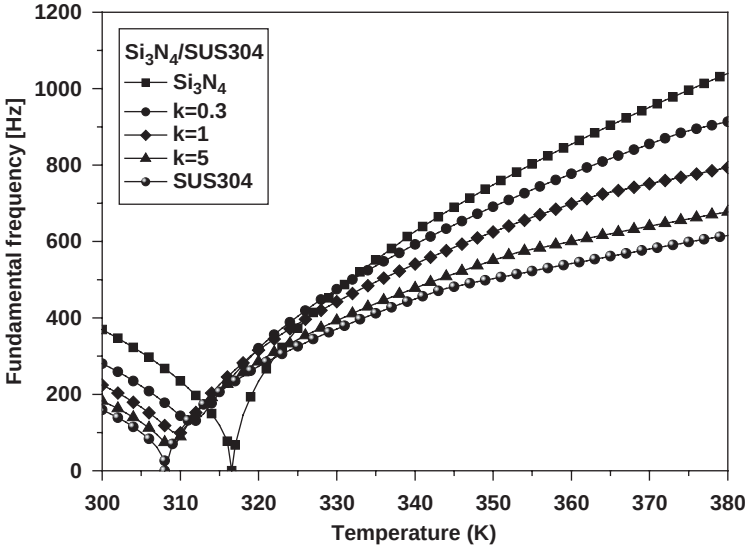

Fig. 8. Vibration behavior of the Si_3N_4/SUS304 FG plate.

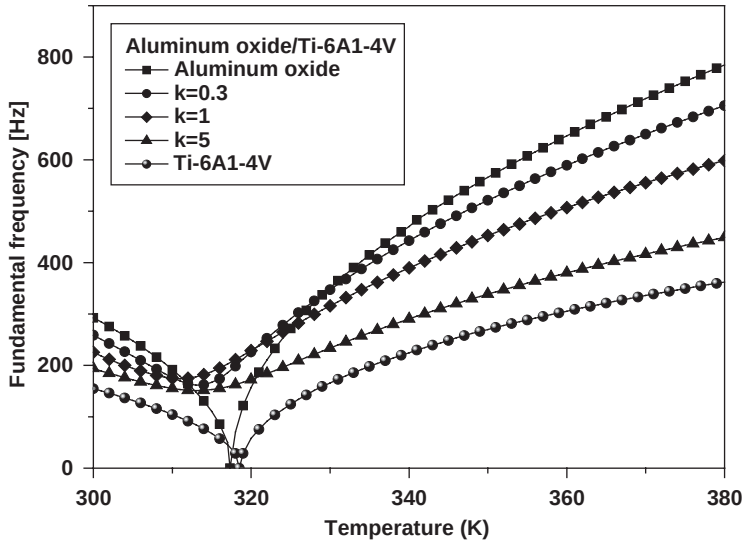

Fig. 9. Vibration behavior of the aluminum oxide/Ti-6A1-4V FG plate.

For the isotropic plates with Si_3N_4, SUS304, aluminum oxide and Ti-6A1-4V, the fundamental frequencies go to zero as the temperature approaches the critical temperature as shown in Figs. 8 and 9. However, fundamental frequencies of the FG plate do not go to zero because the thermal postbuckling behavior of the FG plate is not the bifurcation buckling behavior. In addition, for both the isotropic and the FG plates, as the temperature is increased, fundamental frequencies have decreased in the pre-buckled region, but increased in the postbuckled region, because the

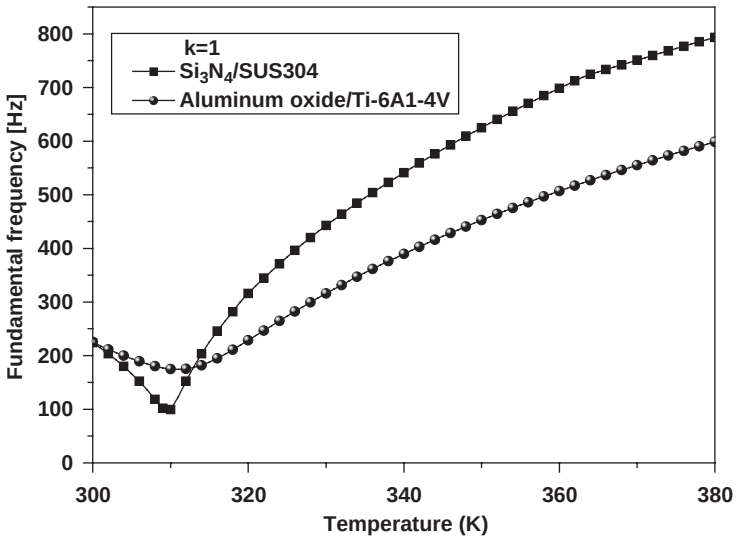

Fig. 10. Vibration behaviors of the Si_3N_4/SUS304 and aluminum oxide/Ti-6A1-4V FG plates with $k = 1$.

thermal large deflection increases the nonlinear stiffness of the plate. At the reference temperature, there are fundamental frequencies of the FG plates between those of the isotropic plates with two constituent isotropic materials, and the larger the volume fraction index for the ceramic k, the smaller fundamental frequency of the FG plate. The temperature–frequency relationship for the aluminum oxide/Ti-6A1-4V FG plate is more monotonic than that for the Si_3N_4/SUS304 FG plate.

Fig. 10 shows the vibration behaviors of the Si_3N_4/SUS304 and aluminum oxide/Ti-6A1-4V FG plates for $k = 1$. In the pre-buckled state, the fundamental frequency of the aluminum oxide/Ti-6A1-4V FG plate is higher than that of the Si_3N_4/SUS304 FG plate, however, in the postbuckled region, the fundamental frequency of the aluminum oxide/Ti-6A1-4V FG plate is lower than that of the Si_3N_4/SUS304 FG plate. This is because the thermal postbuckling deflection of the Si_3N_4/SUS304 FG plate is larger than that of the aluminum oxide/Ti-6A1-4V FG plate.

5. Conclusions

This study represents characteristics of the thermal postbuckling and vibration of the FG plate under thermal loads. For the numerical analysis, the nonlinear finite element equation based on the first-order shear deformation plate theory is formulated, and the incremental method for considering the initial displacement and initial stress is adopted to account for the nonlinear temperature-dependent material properties of FGMs. The numerical results show that the behaviors of the thermal postbuckling and vibration of the FG plate are different from those of the isotropic plate, and the volume fraction of the constituent materials for FGMs has an effect on the behaviors of the thermal postbuckling and vibration of the FG plate. In addition, the behaviors of the FG plate do not necessarily lie in between those of the isotropic plates with the

ceramic and metal. For the future study, the behavior of the FG structure under various temperature distributions will be researched.

Acknowledgement

This work was supported by the Brain Korea 21 project in 2004.

Appendix A

The stiffness matrices and load vectors in Section 2.5 can be derived as follows. By using Eqs. (1), (2), (5) and (6), the variation of the internal virtual work δW_{int} is represented as

$$
\begin{aligned}
\delta W_{\text{int}} &= \int_A [\delta\boldsymbol{\varepsilon}^{\mathrm{T}}\mathbf{N} + \delta\boldsymbol{\kappa}^{\mathrm{T}}\mathbf{M} + \delta\boldsymbol{\gamma}^{\mathrm{T}}\mathbf{Q}]\,\mathrm{d}A \\
&= \int_A \big[(\delta\boldsymbol{\varepsilon}_m^{\mathrm{T}} + \delta\boldsymbol{\varepsilon}_\theta^{\mathrm{T}} + \delta\boldsymbol{\varepsilon}_0^{\mathrm{T}})(\mathbf{A}\Delta\boldsymbol{\varepsilon} + \mathbf{B}\Delta\boldsymbol{\kappa} - \mathbf{N}_{\Delta T} + \mathbf{N}_0) \\
&\quad + \delta\boldsymbol{\kappa}^{\mathrm{T}}(\mathbf{B}\Delta\boldsymbol{\varepsilon} + \mathbf{D}\Delta\boldsymbol{\kappa} - \mathbf{M}_{\Delta T} + \mathbf{M}_0) + \delta\boldsymbol{\gamma}^{\mathrm{T}}(\mathbf{A}_s\Delta\boldsymbol{\gamma} + \mathbf{Q}_0)\big]\,\mathrm{d}A \\
&= \int_A \big[(\delta\boldsymbol{\varepsilon}_m^{\mathrm{T}} + \delta\boldsymbol{\varepsilon}_\theta^{\mathrm{T}} + \delta\boldsymbol{\varepsilon}_0^{\mathrm{T}})(\mathbf{A}\Delta\boldsymbol{\varepsilon}_m + \mathbf{A}\Delta\boldsymbol{\varepsilon}_\theta + \mathbf{A}\Delta\boldsymbol{\varepsilon}_0 + \mathbf{B}\Delta\boldsymbol{\kappa} - \mathbf{N}_{\Delta T} + \mathbf{N}_0) \\
&\quad + \delta\boldsymbol{\kappa}^{\mathrm{T}}(\mathbf{B}\Delta\boldsymbol{\varepsilon}_m + \mathbf{B}\Delta\boldsymbol{\varepsilon}_\theta + \mathbf{B}\Delta\boldsymbol{\varepsilon}_0 + \mathbf{D}\Delta\boldsymbol{\kappa} - \mathbf{M}_{\Delta T} + \mathbf{M}_0) \\
&\quad + \delta\boldsymbol{\gamma}^{\mathrm{T}}(\mathbf{A}_s\Delta\boldsymbol{\gamma} + \mathbf{Q}_0)\big]\,\mathrm{d}A \\
&= \underbrace{\int_A [\delta\boldsymbol{\varepsilon}_m^{\mathrm{T}}\mathbf{A}\Delta\boldsymbol{\varepsilon}_m + \delta\boldsymbol{\varepsilon}_m^{\mathrm{T}}\mathbf{B}\Delta\boldsymbol{\kappa} + \delta\boldsymbol{\kappa}^{\mathrm{T}}\mathbf{B}\Delta\boldsymbol{\varepsilon}_m + \delta\boldsymbol{\kappa}^{\mathrm{T}}\mathbf{D}\Delta\boldsymbol{\kappa} + \delta\boldsymbol{\gamma}^{\mathrm{T}}\mathbf{A}_s\Delta\boldsymbol{\gamma}]\,\mathrm{d}A}_{\mathbf{K}} \\
&\quad + \underbrace{\int_A [\delta\boldsymbol{\varepsilon}_m^{\mathrm{T}}\mathbf{A}\Delta\boldsymbol{\varepsilon}_\theta + \delta\boldsymbol{\varepsilon}_\theta^{\mathrm{T}}\mathbf{A}\Delta\boldsymbol{\varepsilon}_m + \delta\boldsymbol{\varepsilon}_\theta^{\mathrm{T}}\mathbf{B}\Delta\boldsymbol{\kappa} + \delta\boldsymbol{\kappa}^{\mathrm{T}}\mathbf{B}\Delta\boldsymbol{\varepsilon}_\theta]\,\mathrm{d}A}_{\frac{1}{2}\mathbf{KN1}} \\
&\quad + \underbrace{\int_A [\delta\boldsymbol{\varepsilon}_\theta^{\mathrm{T}}\mathbf{A}\Delta\boldsymbol{\varepsilon}_\theta]\,\mathrm{d}A}_{\frac{1}{3}\mathbf{KN2}} - \underbrace{\int_A [\delta\boldsymbol{\varepsilon}_\theta^{\mathrm{T}}\mathbf{N}_{\Delta T}]\,\mathrm{d}A}_{\mathbf{K}_{\Delta T}} + \underbrace{\int_A [\delta\boldsymbol{\varepsilon}_\theta^{\mathrm{T}}\mathbf{N}_0]\,\mathrm{d}A}_{\mathbf{K}_0} \\
&\quad + \underbrace{\int_A [\delta\boldsymbol{\varepsilon}_m^{\mathrm{T}}\mathbf{A}\Delta\boldsymbol{\varepsilon}_0 + \delta\boldsymbol{\varepsilon}_\theta^{\mathrm{T}}\mathbf{A}\Delta\boldsymbol{\varepsilon}_0 + \delta\boldsymbol{\varepsilon}_0^{\mathrm{T}}\mathbf{A}\Delta\boldsymbol{\varepsilon}_m + \delta\boldsymbol{\varepsilon}_0^{\mathrm{T}}\mathbf{A}\Delta\boldsymbol{\varepsilon}_\theta]\,\mathrm{d}A}_{\frac{1}{2}\mathbf{KN1}_{w0}} \\
&\quad + \underbrace{\int_A [\delta\boldsymbol{\varepsilon}_0^{\mathrm{T}}\mathbf{A}\Delta\boldsymbol{\varepsilon}_0 + \delta\boldsymbol{\varepsilon}_0^{\mathrm{T}}\mathbf{B}\Delta\boldsymbol{\kappa} + \delta\boldsymbol{\kappa}^{\mathrm{T}}\mathbf{B}\Delta\boldsymbol{\varepsilon}_0]\,\mathrm{d}A}_{\mathbf{K}_{w0}}
\end{aligned}
$$

$$
\begin{aligned}
&- \underbrace{\int_A [\delta\boldsymbol{\varepsilon}_m^{\mathrm{T}}\mathbf{N}_{\Delta T} + \delta\boldsymbol{\kappa}^{\mathrm{T}}\mathbf{M}_{\Delta T}]\,\mathrm{d}A}_{\mathbf{P}_{\Delta T}} + \underbrace{\int_A [\delta\boldsymbol{\varepsilon}_m^{\mathrm{T}}\mathbf{N}_0 + \delta\boldsymbol{\kappa}^{\mathrm{T}}\mathbf{M}_0 + \delta\boldsymbol{\gamma}^{\mathrm{T}}\mathbf{Q}_0]\,\mathrm{d}A}_{\mathbf{P}_0} \\
&- \underbrace{\int_A [\delta\boldsymbol{\varepsilon}_0^{\mathrm{T}}\mathbf{N}_{\Delta T}]\,\mathrm{d}A}_{\mathbf{P}_{w0_{\Delta T}}} + \underbrace{\int_A [\delta\boldsymbol{\varepsilon}_0^{\mathrm{T}}\mathbf{N}_0]\,\mathrm{d}A}_{\mathbf{P}_{0_{w0}}} \\
&= \delta\mathbf{d}^{\mathrm{T}}(\mathbf{K} - \mathbf{K}_{\Delta T} + \mathbf{K}_0 + \mathbf{K}_{w0} + \tfrac{1}{2}\mathbf{KN1}_{w0} + \tfrac{1}{2}\mathbf{KN1} + \tfrac{1}{3}\mathbf{KN2})\Delta\mathbf{d} \\
&\quad - \delta\mathbf{d}^{\mathrm{T}}\mathbf{P}_{\Delta T} + \delta\mathbf{d}^{\mathrm{T}}\mathbf{P}_0 - \delta\mathbf{d}^{\mathrm{T}}\mathbf{P}_{w0_{\Delta T}} + \delta\mathbf{d}^{\mathrm{T}}\mathbf{P}_{0_{w0}}. \qquad \text{(A.1)}
\end{aligned}
$$

References

[1] J.N. Reddy, Analysis of functionally graded plates, *International Journal for Numerical Methods in Engineering* 47 (2000) 663–684.

[2] L.D. Croce, P. Venini, Finite elements for functionally graded Reissner–Mindlin plates, *Computer Methods in Applied Mechanics and Engineering* 193 (2004) 705–725.

[3] G.N. Praveen, J.N. Reddy, Non-linear transient thermoelastic analysis of functionally graded cerami-metal plates, *International Journal of Solids and Structures* 33 (1998) 4457–4476.

[4] J.R. Cho, J.T. Oden, Functionally graded material: a parametric study on thermal-stress characteristics using the Crank–Nicolson–Galerkin scheme, *Computer Methods in Applied Mechanics and Engineering* 188 (2000) 17–38.

[5] J. Woo, S.A. Meguid, Non-linear analysis of functionally graded plates and shallow shells, *International Journal of Solids and Structures* 38 (2001) 7409–7421.

[6] J. Yang, H.-S. Shen, Non-linear bending analysis of shear deformable functionally graded plates subjected to thermo-mechanical loads under various boundary conditions, *Composites: Part B* 34 (2003) 103–115.

[7] R. Javaheri, M.R. Eslami, Thermal buckling of functionally graded plates, *AIAA Journal* 40 (2002) 162–169.

[8] W. Lanhe, Thermal buckling of a simply-supported moderately thick rectangular FGM plate, *Composite Structures* 64 (2004) 211–218.

[9] K.-S. Na, J.-H. Kim, Three-dimensional thermal buckling analysis of functionally graded materials, *Composites: Part B* 35 (2004) 429–437.

[10] S.S. Vel, R.C. Batra, Three-dimensional exact solution for the vibration of functionally graded rectangular plates, *Journal of Sound and Vibration* 272 (2004) 703–730.

[11] S.C. Pradhan, C.T. Loy, K.Y. Lam, J.N. Reddy, Vibration characteristics of functionally graded cylindrical shells under various boundary conditions, *Applied Acoustics* 61 (2000) 111–129.

[12] J. Yang, H.-S. Shen, Vibration characteristics and transient response of shear-deformable functionally graded plates in thermal environments, *Journal of Sound and Vibration* 255 (2002) 579–602.

[13] S. Kitipornchai, J. Yang, K.M. Liew, Semi-analytical solution for nonlinear vibration of laminated FGM plates with geometric imperfections, *International Journal of Solids and Structures* 41 (2004) 2235–2257.

[14] J. Yang, K.M. Liew, S. Kitipornchari, Dynamic stability of laminated FGM plates based on higher-order shear deformation theory, *Computational Mechanics* 33 (2004) 305–315.

[15] X.Q. He, T.Y. Ng, S. Sivashanker, K.M. Liew, Active control of FGM plates with integrated piezoelectric sensors and actuators, *International Journal of Solids and Structures* 38 (2001) 1641–1655.

[16] K.M. Liew, J. Yang, S. Kitipornchari, Postbuckling of piezoelectric FGM plates subject to thermo-electro-mechanical loading, *International Journal of Solids and Structures* 40 (2003) 3869–3892.

[17] R.C. Averill, J.N. Reddy, Thermomechanically postbuckling analysis of laminated composite shells, *Proceedings of the 34th AIAA/ASME/ASCE/AHS/ASC Structures, Structural Dynamics and Materials Conference*, AIAA-93-1337-CP, 1993, pp. 351–360.

[18] R.C. Zhou, D.Y. Xue, C. Mei, Vibration of thermally buckled composite plates with initial deflections using triangular elements, *Proceedings of the 34th AIAA/ASME/ ASCE/AHS/ASC Structures*, *Structural Dynamics and Materials Conference*, AIAA-93-1321-CP, 1993, pp. 226–235.
[19] D.M. Lee, I. Lee, Vibration behaviors of thermally postbuckled anisotropic plates using first-order shear deformable plate theory, *Computers and Structures* 63 (1997) 371–378.
[20] J.-S. Park, J.-H. Kim, S.-H. Moon, Vibration of thermally post-buckled composite plates embedded with shape memory alloy fibers, *Composite Structures* 63 (2004) 179–188.